Proceedings of the 2012 3rd Micro/Nanoscale Heat & Mass Transfer International Conference
MNHMT2012
March 3-6, 2012, Atlanta, Georgia, USA

MNHMT2012-75266

CONVECTION, EVAPORATION, AND CONDENSATION OF SIMPLE AND BINARY FLUIDS IN CONFINED GEOMETRIES

Tongran Qin
tongran@gatech.edu

Roman O. Grigoriev
romgrig@gatech.edu

George W. Woodruff School of Mechanical Engineering, Georgia Institute of Technology
Atlanta, GA USA 30332-0405

School of Physics, Georgia Institute of Technology
Atlanta, GA USA 30332-0430

ABSTRACT

Rayleigh-Bénard and Marangoni convection in a layer of a homogeneous fluid with a free surface in the absence of phase change is a classic (and extensively studied) problem of fluid mechanics. Phase change has a major effect on the convection problem. Most notably, significant latent heat generated at the free surface as a result of phase change can dramatically alter the interfacial temperature, and hence, the thermocapillary stresses. Furthermore, differential evaporation in binary fluids can lead to considerable variation in the concentration field, producing solutocapillarity stresses, which can compete with thermocapillarity and buoyancy.

This talk describes numerical studies of convection in alcohol and alcohol-water mixtures due to a horizontal temperature gradient in the presence of phase change. We illustrate how the composition of the liquid and the presence of non-condensable gases (e.g., air) can be used to alter the balance of the dominant forces. In particular, by adding or removing air from the test cell, the direction of the flow can be reversed by emphasizing either the thermocapillary or the solutocapillary stresses.

INTRODUCTION

Thermal management is a major issue for a wide range of applications. Evaporative cooling, which exploits the large latent heats associated with phase change, can help with developing lightweight, compact and efficient cooling technologies that can handle very high heat fluxes. However, our fundamental understanding of thermal and mass transport remains limited.

Accurate modeling of surface physics is paramount for proper description of heat and mass transfer in two-phase systems. Phase change (evaporation and condensation) taking place at the liquid-vapor interface tends to determine the pattern of heat flux in the system since large latent heat absorbed or released during phase change can far exceed conductive and convective heat fluxes in the liquid, and especially vapor, phase. Similarly, surface tension forces arising at the liquid-vapor interface tend to dominate body forces such as gravity and buoyancy at small length scales.

For the vast majority of single-component coolants, surface tension decreases as temperature increases, resulting in thermocapillary stresses that drive the liquid away from hot regions, leading to film dryout, for example. However, a number of binary "self-rewetting fluids" consisting of mixtures of long-chain alcohols with water have surface tensions that increase with temperature, leading to thermocapillary stresses that drive liquid towards hot regions, improving cooling performance. Moreover, all binary coolants, self-rewetting or not, are subject to solutocapillary stresses: differential evaporation of the two components with different volatility leads to variation in the local composition of the liquid at the free surface, and hence in surface tension. The flow of liquid can be affected by other physical processes as well. For instance, the flow of vapor from hot to cold regions, especially in slender confined geometries, can produce substantial surface stresses on the liquid. Buoyancy effects can also be non-negligible, especially in the thicker liquid or vapor layers.

In practice it may be very hard to quantify the contribution of different physical mechanisms, since heat and mass transfer are inter-related, often in rather subtle ways. For instance, evaporation and condensation can greatly change the local temperature, and hence the thermocapillary stresses, along the liquid-vapor interface. Similarly, the presence of noncondensable gases, such as air, can radically alter the transport of coolant vapors towards and away from the interface, profoundly modifying the liquid composition and the associated solutocapillary stresses.

This makes comprehensive numerical models invaluable for our fundamental understanding of transport processes. The vast majority of existing models, however, are only applicable to highly idealized geometries (e.g., immediate vicinity of apparent contact lines [1],[2],[3], high-aspect-ratio channels in heat-pipe applications [4],[5][6], near-spherical liquid-vapor interfaces in nucleate boiling [7], etc.). Very few studies include detailed models of the vapor phase [8],[9] and even fewer consider the effects of non-condensable gases such as air [10] which, as we demonstrate below, can be rather dramatic. Models that are capable of treating binary liquids are also rare [7],[11],[12]. There are no models that, at the same time, are capable of describing arbitrary geometries, both simple and binary liquids, and provide detailed description of both the liquid and the vapor phase.

Below we introduce such a detailed numerical model that provides a comprehensive and quantitative description of heat and mass transport in arbitrary confined geometries. We also illustrate the physical insights that can be obtained with the help of this model for a canonical problem – a two-phase system in a rectangular cavity driven out of thermodynamic equilibrium by imposing a horizontal temperature gradient.

MATHEMATICAL MODEL

Governing Equations

Both the liquid and the vapor phase can be considered incompressible since the fluid velocities $\mathbf{u}$ are much smaller than the speed of sound at small length scales, so the continuity equation reduces to $\nabla \cdot \mathbf{u} = 0$. Because the fluid velocities can, however, be large enough for inertial effects to be significant, the momentum transport in the bulk is described by the Navier-Stokes equation

$$\rho(\partial_t \mathbf{u} + \mathbf{u} \cdot \nabla \mathbf{u}) = -\nabla p + \mu \nabla^2 \mathbf{u} + \rho(T)\mathbf{g} \tag{1}$$

where p is the fluid pressure, ρ and μ are the fluid's density and viscosity, and $\mathbf{g}$ is the gravitational acceleration. We used the Boussinesq approximation, retaining the temperature dependence only in the last term to retain the buoyancy force. This is consistent with the assumption of incompressibility, since the relative change in the density due to temperature variation is usually quite small (about 3% for the vapor, 1.5% for the liquid in the examples considered below). The heat transport is described using an advection-diffusion equation

$$\partial_t T + \mathbf{u} \cdot \nabla T = \kappa \nabla^2 T \tag{2}$$

where $\kappa = k/\rho C_p$ is the fluid thermal diffusivity (k is the thermal conductivity, and C_p is the heat capacity, of the fluid). The liquids are considered to be incompressible, with density

$$\rho_l^n = \rho_l^{n,0}[1 - \alpha_l^n (T - T_0)] \tag{3}$$

where $\alpha_l^n = -(\partial \rho_l^n / \partial T)/\rho_l^{n,0}$ is the coefficient of thermal expansion (here and below, superscripts denote different components in mixtures, while subscripts denote the phases). The vapors are considered to be ideal gases

$$p_v^n = \rho_v^n \bar{R}^n T \tag{4}$$

where $\bar{R}^n = R/M^n$, R is the universal gas constant, and M^n is the molar mass. Both equations of state (3) and (4) can be easily generalized as needed.

The Navier-Stokes equation only describes simple fluids or multi-component fluids in the dilute approximation. Although the equations governing momentum transport in multi-component mixtures generalizing the Navier-Stokes equation for a simple fluid are known [13], no efficient numerical solvers for these equations have been developed. Hence, we restrict the model to situations when the dilute approximation is valid in both the liquid and the vapor phase, i.e., the molar fraction of one component (denoted with superscript d below) is much greater than that of the other(s). Conventionally, the mass transport of the less abundant components is described by the advection-diffusion equation for concentration. However, this equation does not guarantee mass conservation, which becomes a serious problem in confined geometries. To ensure local mass conservation, we use the advection-diffusion equation for the density instead,

$$\partial_t \rho^n + \mathbf{u} \cdot \nabla \rho^n = D^n \nabla^2 \rho^n, \quad n \neq d \tag{5}$$

where D^n is the diffusion coefficient of component n in the dominant component d. As a consequence, the mass of all components $n \neq d$ is also conserved globally.

Mass conservation of the dominant component requires a separate equation

$$\int_{\text{vapor}} \rho_v^d \, dV + \int_{\text{liquid}} \rho_l^d \, dV = m^d \tag{6}$$

where m^d is its total mass. Since the liquids are incompressible, the densities ρ_l^n of different components in the multicomponent liquid are related via

$$\sum_n \frac{\rho_l^n}{\bar{\rho}_l^n} = 1 \tag{7}$$

where $\bar{\rho}_l^n$ are the densities of pure components, allowing ρ_l^d to be expressed via $\rho_l^{n\neq d}$. The density of the dominant component in the vapor phase is

$$\rho_v^d = \frac{p_v^d}{\bar{R}^d T} \tag{8}$$

while its partial pressure is related to the total pressure via

$$p_v^d = p_v - \sum_{n\neq d} p_v^n \tag{9}$$

and the partial pressures $p_v^{n\neq d}$ of other components are computed from $\rho_v^{n\neq d}$ using (4). Finally, the solution of the Navier-Stokes equation defines the pressure field p only up to a constant p_o, so that total pressure is

$$p_v = p + p_o \tag{10}$$

The pressure offset p_o can therefore be computed from the mass conservation constraint (6) using (7), (8), (9), and (10).

It should be emphasized that different components could be dominant in the liquid phase and in the vapor phase. For example, for a water-methanol mixture under air at atmospheric pressure, air is dominant in the vapor phase, while water (or methanol) is dominant in the liquid phase. Since total pressure only affects the density of vapor components, (6) applies to the component which is dominant in the vapor phase. In particular, if a noncondensable gas is dominant in the vapor, the second term on the left-hand-side of (6) vanishes, since $\rho_l^d = 0$.

The concentration (or molar fraction) c_v^n of different components in the vapor can be computed from the equation of state using their partial pressures

$$c_v^n = p_v^n / p_v \tag{11}$$

while in the liquid

$$c_l^n = \frac{\rho_l^n / \mathrm{M}^n}{\sum_n (\rho_l^n / \mathrm{M}^n)} \tag{12}$$

The dilute approximation implies $c^{n\neq d} \ll c^d = 1 - \sum_{n\neq d} c^n$.

Boundary Conditions

The system of coupled evolution equations for the velocity, pressure, temperature, and density fields has to be solved in a self-consistent manner, subject to the boundary conditions discussed below. The phase change for binary mixtures is described using expressions for the mass flux of each component across the liquid-vapor interface

$$J^n = 2\rho_v^n \sqrt{\frac{\bar{R}^n T_i}{2\pi}} \left[\frac{p_l - p_v}{\rho_l^n \bar{R}^n T_{\mathrm{sat}}^n} + \frac{\bar{h}_{lv}^n}{\bar{R}^n T_{\mathrm{sat}}^n} \frac{T_i - T_{\mathrm{sat}}^n}{T_{\mathrm{sat}}^n} \right] \tag{13}$$

based on Kinetic Theory [14], where subscript i indicates values at the liquid-vapor interface. Unlike the standard expression for simple fluids [1], for mixtures, besides the latent heat of phase change, (13) also includes the contribution from the mixing entropy. For binary liquids

$$\bar{h}_{lv}^n = h_{lv}^n - RT_i[c_1 \ln c_1 + c_2 \ln c_2] \tag{14}$$

The saturation temperature for each component is computed from Antoine's equation

$$\log_{10} p_{\mathrm{sat}}^n = A^n - \frac{B^n}{C^n + T_{\mathrm{sat}}^n} \tag{15}$$

with empirical coefficients A^n, B^n, and C^n, where local thermodynamic equilibrium is assumed to relate saturation pressure p_{sat}^n to the vapor density and concentration on the liquid side:

$$c_l^n p_{\mathrm{sat}}^n = \rho_v^n \bar{R}_n T_i \tag{16}$$

The heat flux balance is given by

$$\sum_n \bar{h}_{lv}^n J^n = k_l \mathbf{n} \cdot \nabla T_l - k_v \mathbf{n} \cdot \nabla T_v \tag{17}$$

The remaining boundary conditions for $\mathbf{u}$ and T at the liquid-vapor interface are standard: the continuity of the temperature $T_l = T_v$ and tangential component of the velocity $(1 - \mathbf{n}\cdot\mathbf{n})(\mathbf{u}_l - \mathbf{u}_v) = 0$. Mass balance gives

$$\rho_l \mathbf{n} \cdot (\mathbf{u}_l - \mathbf{u}_i) = \rho_v \mathbf{n} \cdot (\mathbf{u}_v - \mathbf{u}_i) = \sum_n J^n \tag{18}$$

in the absence of noncondensable gases. In the opposite limit, when noncondensables dominate the gas mixture, the vapor-side boundary condition is modified to $\mathbf{n} \cdot (\mathbf{u}_v - \mathbf{u}_i) = 0$. The stress balance can be written as

$$(\Sigma_l - \Sigma_v) \cdot \mathbf{n} = \mathbf{n}\sigma + \nabla_s \sigma \tag{19}$$

where $\Sigma = \mu[\nabla\mathbf{u} - (\nabla\mathbf{u})^T] - p$ is the stress tensor and $\nabla_s = (1 - \mathbf{n}\cdot\mathbf{n})\nabla$ is the surface gradient. In the binary liquid mixture, the surface tension is $\sigma = \sigma^1 c_l^1 + \sigma^2 c_l^2$ where we assume linear temperature dependence $\sigma^n \approx \sigma_0^n + \sigma_1^n (T - T_0)$ for both components. For $c_l^1 \gg c_l^2$ (e.g., $d = 1$) the stress balance boundary condition (19) reduces to

$$(\Sigma_l - \Sigma_v) \cdot \mathbf{n} \approx \mathbf{n}\sigma_0^1 + \sigma_1^1 \nabla_s T + (\sigma_0^2 - \sigma_0^1) \nabla_s c_l^2 \tag{20}$$

and incorporates the viscous drag between the two phases, the thermo- and solutocapillary effects, as well as the capillary pressure.

The boundary conditions for the density fields at the liquid-vapor interface were derived from the expressions for the

mass flux. In particular, the density gradient in binary liquids can be computed with the help of the incompressibility condition and mass conservation, yielding

$$\mathbf{n}\cdot\nabla\rho_l^2 = \frac{r[(mJ^1+J^2)c_l^2 - J^2]}{D_l^2(1-c_l^2)} \tag{21}$$

where $m = M^2/M^1$ and $r = \bar{\rho}_l^2/\bar{\rho}_l^1$.

The boundary conditions on the vapor side depend on the presence of noncondensable gases. For instance, in the presence of air at atmospheric pressure, the transport of vapor towards and away from the interface, for both simple and binary liquids, is greatly impeded by diffusion, so one can assume vapor densities to be equal to the equilibrium values given by (15) and (16) with

$$T_{\text{sat}}^n = \mathrm{T}_i\left[1 - \frac{p_l - p_v}{\rho_l^n \bar{h}_{lv}^n}\right]^{-1} \approx \mathrm{T}_i \tag{22}$$

Although the last expression is a solution of (13) with $J^n = 0$, the mass fluxes do not vanish exactly and can be computed from the density and the gradient of concentration in the vapor phase

$$J^n = -\rho_v^n D_v^n \mathbf{n}\cdot\nabla c_v^n \tag{23}$$

Similarly, in the absence of non-condensable gases, for binary liquids whose vapors can be treated in the dilute approximation, the transport of the less abundant component (here $n = 2$) is impeded by diffusion in the dominant component, so its density ρ_v^n and concentration c_v^n should also be computed using (15), (16), and (22) and its mass flux using (23), rather than directly from (13).

IMPLEMENTATION

The model described above has been implemented numerically by adapting a commercially available open-source CFD package OpenFOAM [15] to solve the governing equations in both 2D and 3D geometries.

Each time step involves three major parts: updating the interface shape and the computational mesh; updating the boundary conditions on the velocity, pressure, temperature and density fields; and updating pressure, velocity, temperature, density and concentration fields in the bulk. Since the interface shape, the boundary conditions, and the bulk fields are coupled, these three parts are repeated iteratively, until convergence.

The shape of the liquid-vapor interface is updated using (18) based on the velocity u_l in the liquid phase. We use the surface tracking method [16] in which the interface coincides with a set of mesh cell faces. Since the computational mesh has to conform to the interface shape at all times, it is being continuously distorted by the interface motion.

In order to solve the governing equations for the bulk fields in the liquid and the vapor domain, the boundary conditions are updated on both sides of the interface. Since the mass flux(es) J^n, the interfacial temperature T_i and the equilibrium density field(s) ρ^n are coupled, the corresponding boundary conditions are also computed iteratively.

Boundary conditions also need to be updated on all the solid walls, since calculations are carried out in confined geometries. No-slip boundary condition is used for the velocity; pressure boundary condition $\mathbf{n}\cdot\nabla p = \rho\mathbf{n}\cdot\mathbf{g}$ follows from (1); temperature is fixed on the outside of heated or cooled walls, and vanishing heat flux is imposed on all other walls which are considered adiabatic; no-flux boundary condition for the density is used on all walls. The types of boundary conditions are summarized in Table 1. For instance, temperature continuity is imposed on the vapor side, while the heat flux balance (17) is imposed on the liquid side.

Physical field	Types of boundary conditions			
	Interface		Heated or cooled walls	Other walls
	Vapor side	Liquid side		
U	Dirichlet	Neumann	Dirichlet	Dirichlet
P	Neumann	Dirichlet	Neumann	Neumann
T	Dirichlet	Neumann	Neumann	Neumann
ρ	Dirichlet	Neumann	Neumann	Neumann

Table 1 Types of boundary conditions imposed on various boundaries in the numerical implementation of the model.

Finite volume method [17] is used for calculating pressure, velocity, temperature, density, and concentration fields. In particular, pressure and velocity are solved for using PISO (Pressure Implicit with Splitting of Operators) algorithm [18], where velocity field is predicted before the pressure equation is solved so that continuity is satisfied, and velocity is then corrected based on changes in pressure field. It is an iterative procedure repeated until both the pressure and the velocity field converge. Once velocity field is computed, temperature, density and concentration fields are updated.

RESULTS AND DISCUSSIONS

In this section, we will use the computational model presented above to illustrate the fundamental distinction between the behavior of simple and binary fluids in the same experimental configuration (described in more detail in Ref. [19]). We will also illustrate the dramatic effect that the presence of noncondensable gases can introduce. The basic geometry is shown in Figure 1. A layer of liquid is confined in a sealed rectangular cavity below a layer of vapor, which is either pure vapor or air mixed with vapor. The cavity of inner dimensions 48.5 mm × 10 mm × 10 mm is made of quartz and has 1.25 mm thick walls. External temperature gradient is generated by imposing different temperatures on the outside of the walls at the "cold" and "hot" end, $\mathrm{T_c} = 288$ °K and $\mathrm{T_h} = 298$ °K. A fixed contact angle $\alpha = 60°$ is specified on all solid walls. While the numerical model can simulate both

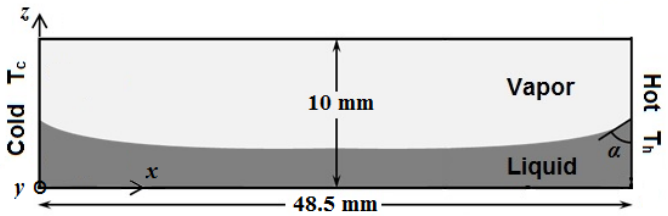

Figure 1 Orthographic views showing longitudinal slice of the basic flow geometry.

2D and 3D systems, we only present the results of 2D simulations here (ignoring variation in the *y*-direction).

In this geometry, the magnitude of the interfacial velocity due to the three main physical effects driving the flow can be estimated using lubrication theory, assuming the liquid layer to be of constant thickness H_l much smaller than the cavity length L. Specifically, for buoyancy-, thermocapillary- and solutocapillary-driven flow, respectively, we obtain

$$u_B = \frac{H_l^3}{48}\frac{\partial_T \rho_l g}{\mu_l L}\Delta T \tag{24}$$

$$u_T = \frac{H_l}{4}\frac{\partial_T \sigma}{\mu_l L}\Delta T_i \tag{25}$$

$$u_S = \frac{H_l}{4}\frac{\partial_c \sigma}{\mu_l L}\Delta c_i \tag{26}$$

where $\Delta T = T_h - T_c$ is the imposed temperature difference on the outside walls of the cavity, ΔT_i is the temperature variation along the interface (which is usually significantly less than ΔT) and Δc_i is the concentration variation along the interface. We use the volume of liquid which corresponds to $H_l = 2.5$ mm.

Unlike u_B, which is about 1 mm/s for all the cases studies here, u_T and u_S cannot be estimated without the knowledge of the temperature and concentration fields, both of which are crucially affected by advection, diffusion, and phase change. In deriving the estimates (24)-(26) we assumed that pressure gradient arises in the liquid layer due to a slight variation in its thickness, resulting in the formation of reverse flow along the bottom of the cavity, such that the total flux of the liquid through any plane normal to the *x*-axis vanishes (or more precisely, is much less than the evaporation/condensation flux). In the limit of $H_l/L \to 0$ (e.g., in micro heat pipes) the total flux of the liquid will be nonzero and the combined effect of hydrostatic and capillary pressure variation will have to be considered as a separate forcing term.

Simple Liquid under Its Own Vapor

The majority of current two-phase cooling devices use simple fluids as coolants. A layer of simple liquid under its own vapor also represents the simplest example of a two-phase system, which makes it a good choice for model validation. The results reported here were obtained for pure methanol. Figure 2 shows the velocity field near the cooled end and near the heated end.

The flow in the vapor phase is dominated by the pressure difference between the hot vapor at the right end of the cavity and the cold vapor at the left end. It is well known that, in the absence of noncondensables, evaporation and condensation primarily take place at or near the contact lines [1]. As Figure 3 illustrates, we find the interfacial temperature to be essentially equal to T_{sat}, except very close to the contact lines [20], where it sharply rises to $T_h^* \approx 294.4$ °K at the hot wall and falls to $T_c^* \approx 292.4$ °K at the cold wall. Indeed, using (13) and (17) it is easy to show that in this case

$$T_i \approx T_{\text{sat}} + O\left(\frac{\delta}{H_l}\Delta T\right) \tag{27}$$

at distances greater than the characteristic length scale

$$\delta = \frac{k_l \bar{R}}{2\rho_v}\left(\frac{T_{\text{sat}}}{\bar{h}_{lv}}\right)^2 \sqrt{\frac{2\pi}{\bar{R}T_{\text{sat}}}} \tag{28}$$

away from the heated/cooled walls, where $\delta \approx 0.12$ μm for methanol. This length scale, as well as the temperature scale $|T_i - T_{\text{sat}}| \sim 5 \times 10^{-4}$ °K obtained from (27), is consistent with the results of numerical simulations presented in Figure 3 which correspond to $\Delta T_i \approx 10^{-3}$ °K. Although our simulations cannot fully resolve temperature variation on length scale as small as δ (the mesh resolution is 30μm), Figure 2 shows that the largest vapor velocities are observed near the contact lines, which confirms the expected localization of the regions where phase change is most intense.

Thermocapillarity is not expected to play a role in this case since ΔT_i is so small. Indeed, we find $u_T \approx 0.002$ mm/s (much less than $u_B \approx 1$ mm/s). The direction and the magnitude of the velocity field in the liquid layer suggest that in this case buoyancy is the dominant force driving the flow in the liquid phase. As Figure 2 shows, warmer liquid near the hot wall rises and cooler liquid near the cold wall sinks, resulting in the flow from the hot to the cold end (with maximal velocities of about 1.7 mm/s, comparable to u_B) along the interface and a return flow along the bottom of the cavity.

Our results for pure methanol are generally consistent with those reported in the heat pipe literature [21], where the cavity contains a simple coolant and its vapor, but no air (or other noncondensables). In particular, we find that the cavity can be separated into three regions in the axial (*x*) direction: the region near the hot wall where most of the evaporation takes place, an adiabatic region in the middle, where the interface has an essentially constant temperature, and the region near the cold wall, where most of the condensation takes place.

Binary Liquid under Its Own Vapor

For most single component liquids, thermocapillary stresses tend to drive the liquid away from the hotter regions of

the interface and towards the colder ones. On the other hand, solutocapillary stresses, which are caused by concentration gradients in binary fluids, even dilute ones, can drive the liquid flow in the opposite direction.

This is illustrated here for a water-methanol mixture under its own vapor. Methanol dominates the composition in both phases: the concentration of water is low in the liquid phase ($c_l^2 \approx 0.1$) and even lower in the vapor phase. As Figure 4 shows, the binary liquid flows in the direction opposite to that of the simple liquid: towards the heated end along the interface and back to the cooled end along the bottom of the cavity. Furthermore, the magnitude of the velocity in the binary liquid is significantly larger than that of the simple fluid (pure methanol) under the same conditions, suggesting that solutocapillary stresses exceed both thermocapillary stresses and buoyancy and are the dominant force in this case.

The variation in the composition of the binary liquid in a thin layer just below the interface is a result of the competition between the differential evaporation and condensation which, respectively, decreases or increases the concentration of the more volatile component relative to its value in the bulk and the molecular diffusion in the liquid which tends to make the concentration uniform. The balance between these competing processes determines the normal component of the concentration gradient in the liquid via (21) and hence the variation Δc_i in the concentration that is established along the interface.

While water-methanol mixture is not self-rewetting (its surface tension decreases with temperature), the variation in the interfacial concentration will cause solutocapillary stresses. Since methanol is more volatile than water, the concentration of water at the interface increases near the heated end and decreases near the cooled end due to differential evaporation of the two components. The surface tension of water (about 73 mN/m) is greater than that of methanol (about 23 mN/m). Therefore, surface tension of the water-methanol mixture is expected to be larger near the heated end than near the cooled end, resulting in solutocapillary stresses which drive the liquid towards the heated end along the interface.

In the absence of noncondensable gases, unimpeded transport of vapor away from or towards the interface produces large differences in the evaporation rates of water and methanol. As Figure 5 shows, this results in significant variation in the liquid composition ($\Delta c_i \approx 0.01$), enhancing solutocapillary effects. On the other hand, the variation of the interfacial temperature is very small (the temperature field for the water-methanol mixture is similar to that shown in Figure 3 for pure methanol, with $\Delta T_i \approx 0.03$ ^{o}K), which suppresses thermocapillary effect. This yields $u_S \approx 11$ mm/s and $u_T \approx 0.05$ mm/s, explaining why adding even a small amount of water to methanol not only reverses the direction of the liquid flow, but also makes the flow substantially stronger, compared with pure methanol. The velocity range in the numerics is comparable to u_S, while $u_T \ll u_B \ll u_S$.

We are not aware of published results that can be directly compared with ours. We find many similarities with the case of heat pipes containing simple coolants and no air (e.g., the cavity can be separated into the evaporator/adiabatic/condenser sections), except for the opposite direction of the liquid flow. Furthermore, we find the flow of binary fluid under its vapor to be unsteady, with convection rolls that slowly drift away from the hot wall. This is similar to hydrothermal waves that form in thermocapillary-driven films [22], however, in the present case the instability is driven by variation of concentration, rather than temperature, at the interface.

The Effects of Noncondensable Gases

Noncondensable gases, such as air, are often present inside two-phase cooling devices. While for small concentrations the effects of noncondensables can be fairly subtle, large amounts of noncondensable gases can completely change the pattern of heat and mass flow. Therefore, understanding their role is crucial for a wide range of heat transfer applications.

In this section we investigate the effects of adding air at atmospheric pressure to the binary liquid considered in the previous Section. When a noncondensable gas, such as air, is dominant in the vapor phase, it greatly impedes the transport of vapors away from/towards the interface, dramatically reducing the corresponding mass fluxes and, with them, the amount of latent heat released/absorbed at the interface. As a result, in the presence of air we can expect significant variation of temperature T_i along the interface (as illustrated by Figure 6), which greatly enhances thermocapillary stresses. Indeed, in this case we find $\Delta T_i \approx 4$ ^{o}K, which yields $u_T \approx 7$ mm/s. On the other hand, we should expect an equally significant reduction in differential evaporation and, therefore, concentration variation and solutocapillary stresses. The concentration of water in the liquid phase is found to be essentially constant. We find $\Delta c_i \approx 10^{-5}$ which yields $u_S \approx 10^{-2}$ mm/s, ranking the physical effects in the opposite order, $u_S \ll u_B \ll u_T$, compared with the case of vapor transport unimpeded by noncondensables.

The computed velocity field in this system is shown in Figure 7. The flow direction (from hot to cold wall along the interface) and the magnitude of velocity is consistent with thermocapillary stresses being the dominant force driving the flow. In a related study [23] employing a self-rewetting fluid (1-heptanol/water mixture) the fluid was observed to flow in the opposite direction (from cold to hot wall along the interface). This is also consistent with thermocapillary stresses being the dominant force, since for self-rewetting fluids surface tension increases with temperature (inverse Marangoni effect).

CONCLUSIONS

Our results demonstrate that thermocapillary and solutocapillary effects often play a dominant role in defining mass and heat transport in confined two-phase flows. In virtually all simple-fluid coolants thermocapillary effects promote film dryout by driving the liquid away from hot spots. Binary fluids, on the other hand, have the potential to enhance thermal performance of evaporative cooling devices via

solutocapillary effects, which drive liquid towards hot spots and reduce film dryout. Our results also suggest that the presence of noncondensables such as air reduces the beneficial solutocapillary effect and enhances the adverse thermocapillary effect by suppressing evaporation and condensation.

In the geometry considered, viscous drag was found to have a relatively minor effect on the liquid flow, compared with buoyancy, solutocapillary, and thermocapillary stresses. This is a consequence of the large thickness of the gas layer compared with the liquid layer and small viscosity of the gas phase compared with the liquid. Nonetheless, buoyancy was found to dominate the flow of simple liquids under their own vapor when latent heat suppresses temperature variation along the interface.

Finally, we should point out that in all cases considered, we observed very significant variation of temperature on solid walls in the vicinity of contact lines, despite the wall material (in our case quartz) having thermal conductivity far exceeding the conductivity of the liquid. This suggests that the use of constant temperature boundary conditions is an assumption that can rarely be justified in practice.

ACKNOWLEDGMENTS

This work is supported by ONR under Grant No. N00014-09-1-0298. We are grateful to Zelko Tukovic and Hrvoje Jasak for help with numerical implementation using OpenFOAM.

REFERENCES

[1] Wayner, P.C. Jr., Kao, Y. K., LaCroix, L. V., 1976, "The Interline Heat Transfer Coefficient of an Evaporating Wetting Film," *Int. J. Heat Mass Trans.* **19**, pp. 487-492.

[2] Stephan, P. C. and Busse, C. A., 1992, "Analysis of the Heat Transfer Coefficient of Grooved Heat Pipe Evaporator Walls," *Int. J. Heat Mass Trans.* **35**, pp. 383-391.

[3] Park, K. and Lee, K.-S., 2003, "Flow and Heat Transfer Characteristics of the Evaporating Extended Meniscus in a Micro-Capillary Channel," *Int. J. Heat Mass Trans.* **46**, pp. 4587-4594.

[4] Ma, H. B. and Peterson, G. P., 1997, "Temperature Variation and Heat Transfer in Triangular Grooves with an Evaporating Film," *J. Thermophys. Heat Tr.* **11**, pp. 90-97.

[5] Sartre, V., Zaghdoudi, M. C. and Lallemand, M., 2000, "Effect of Interfacial Phenomena on Evaporative Heat Transfer in Micro Heat Pipes," *Int. J. Therm. Sci*. **39**, pp. 498-504.

[6] Nilson, R. H., Griffiths, S. K., Tchikanda, S. W. and Martinez, M. J., 2004, "Axially Tapered Microchannels of High Aspect Ratio for Evaporative Cooling Devices," *J. Heat Transfer-T. ASME* **126**, pp. 453-462.

[7] Kern, J. and Stephan, P., 2003, "Theoretical Model for Nucleate Boiling Heat and Mass Transfer of Binary Mixtures," *J. Heat Transfer-T. ASME* **125**, pp. 1106-1115.

[8] Suman, B., Hoda, N., 2007, "On the Transient Analysis of a V-Shaped Microgrooved Heat Pipe," *J. Heat Transfer-T. ASME* **129**, pp. 1584-1591.

[9] Zhang, J., Watson, S. J., Wong, H., 2007, "Fluid Flow and Heat Transfer in a Dual-Wet Micro Heat Pipe," *J. Fluid Mech.* **589**, pp. 1-31.

[10] Wang, H., Murthy, J. Y., Garimella, S. V., 2008, "Transport from a Volatile Meniscus Inside an Open Microtube," *Int. J. Heat Mass Trans.* **51**, pp. 3007-3017

[11] Savino, R. and Paterna, D., 2006, "Marangoni Effect and Heat Pipe Dry-Out," *Phys. Fluids* **18**, 118103.

[12] Wee, S.-K., Kihm, K. D., Pratt, D. M. and Allen J. S., 2006, "Microscale Heat and Mass Transport of Evaporating Thin Film of Binary Mixture," *J. Thermophys. Heat Tr.* **20**, pp. 320-326.

[13] Adkins, J. E., 1963, "Nonlinear Diffusion, I. Diffusion and Flow of Mixtures of Fluids," *Phil. Trans. Roy. Soc. Lond.* **255**, pp. 607-633.

[14] Schrage, R. W., 1953, *A Theoretical Study of Interface Mass Transfer*, Columbia University Press, New York.

[15] http://www.openfoam.com.

[16] Ferziger, J. H. and Peric, M., 1996, *Computational Methods for Fluid Dynamics*, Springer-Verlag, Berlin.

[17] LeVeque, R., 2002, *Finite Volume Methods for Hyperbolic Problems*, Cambridge University Press, Cambridge.

[18] Issa, R. I., 1986, "Solution of the Implicitly Discretised Fluid Flow Equations by Operator-Splitting," *J. Comp. Phys.* 62, pp. 40-65.

[19] Li, Y., Chan, B. M. and Yoda M., "Experimental studies of nonisothermal binary fluids with phase change in confined geometries," ASME paper number MNHMT12-75246.

[20] Morris, S. J. S., 2000, "A Phenomenological Model for the Contact Region of an Evaporating Meniscus on a Superheated Slab," *J. Fluid Mech.* **411**, pp. 59-89.

[21] Sobhan, C. B., Rag, R. L. and Peterson, G. P., 2007, "A Review and Comparative Study of the Investigations on Micro Heat Pipes," *Int. J. Energy Res.* **31**, pp. 664–688.

[22] Smith, M. K., 1986, "Instability Mechanisms in Dynamic Thermocapillary Liquid Layers," *Phys. Fluids* **29**, pp. 3182-3186.

[23] di Francescantonio, N., Savino, R. and Abe Y., 2008, "New Alcohol Solutions for Heat Pipes: Marangoni Effect and Heat Transfer Enhancement," *Int. J. Heat Mass Trans.* **51**, pp. 6199-6207.

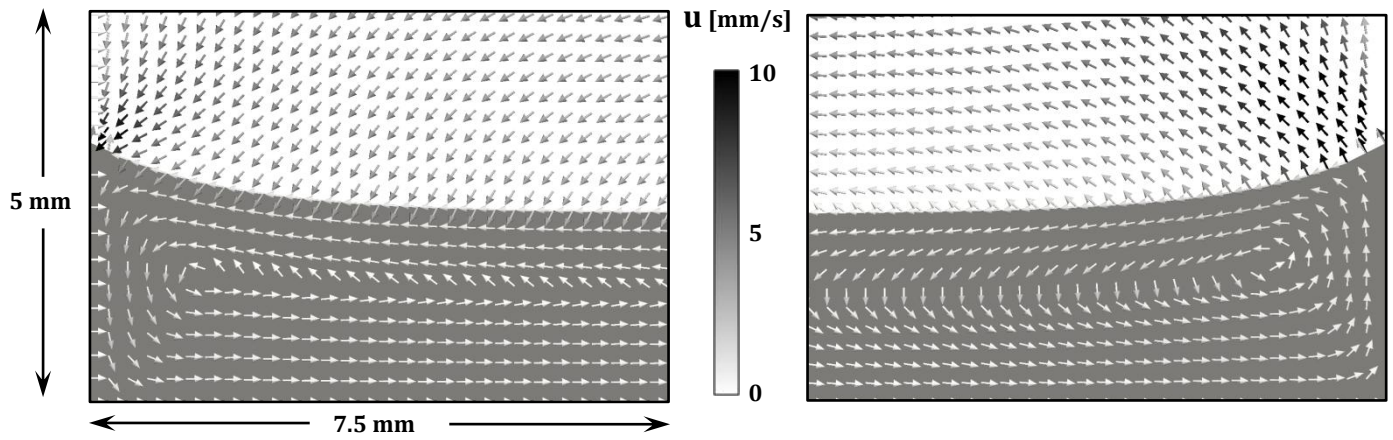

Figure 2 The liquid- and vapor-phase velocity fields for pure methanol under its own vapor. The panels show the cooled [left] and heated [right] ends of the cavity. The gray background indicates liquid, the white background – vapor.

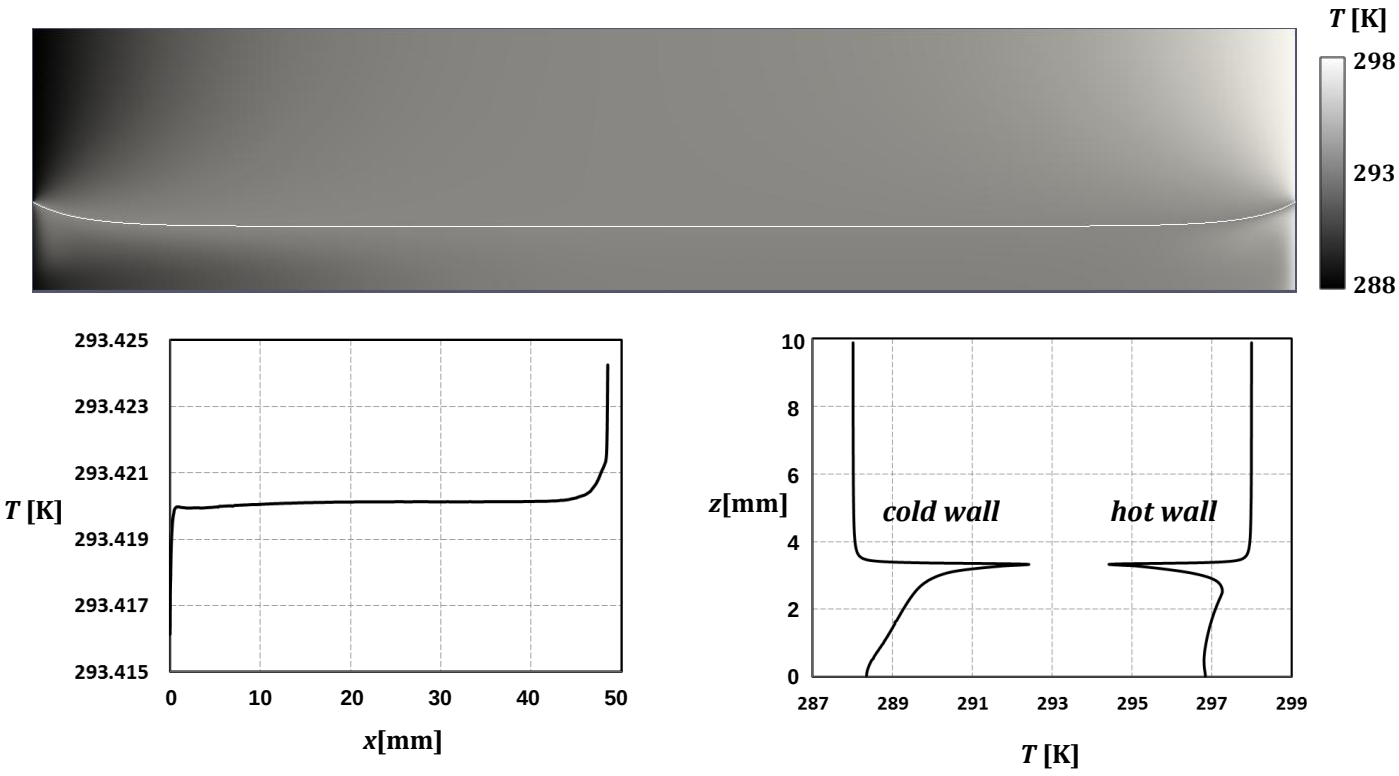

Figure 3 The temperature field for pure methanol under its own vapor. The entire cavity is shown in the upper panel. The thin white line shows the position of the liquid-vapor interface. The temperature distributions along the interface [lower left panel] and along the side walls [lower right panel] are also shown.

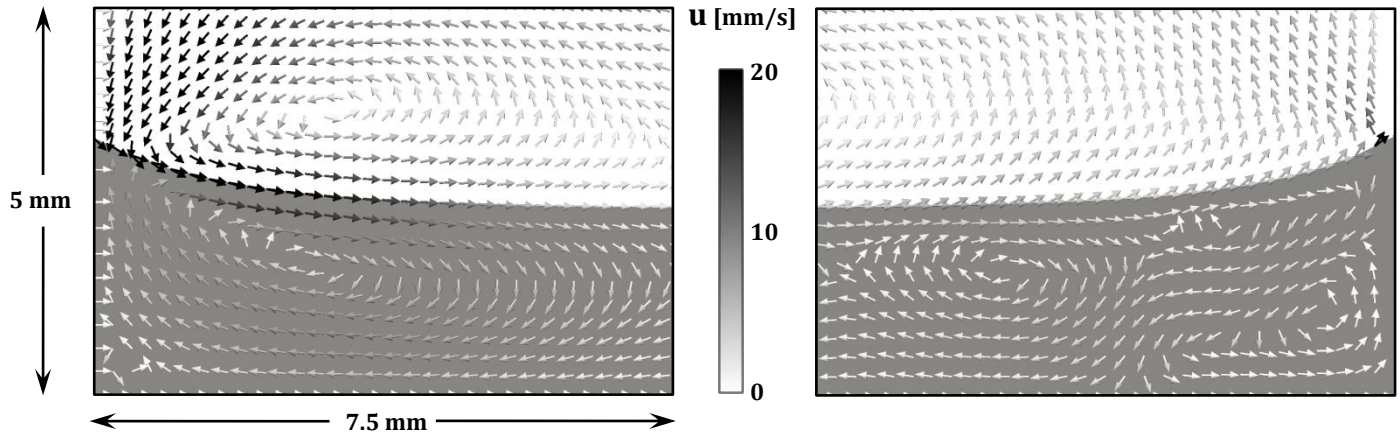

Figure 4 The liquid- and vapor-phase velocity fields for the binary liquid mixture with isothermal composition of 90 mol% methanol and 10 mol% water ($c_l^2 = 0.1$) under its own vapor. The panels show the cooled [left] and heated [right] ends of the cavity. The gray background indicates liquid, the white background – vapor.

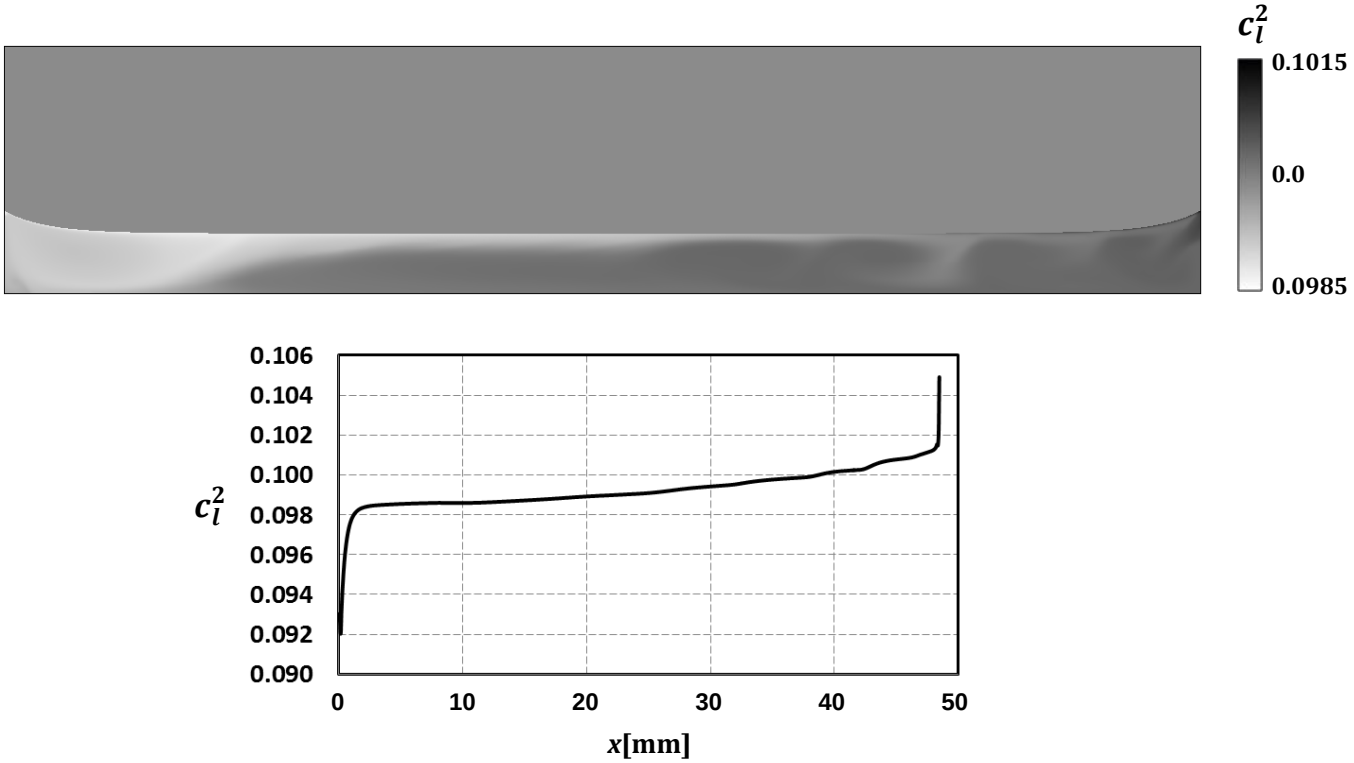

Figure 5 The concentration (molar fraction) of water in the water-methanol binary liquid under its own vapor. The upper panel shows the entire cavity with the concentration field in the vapor phase set to an arbitrary unphysical value. The lower panel shows the variation of the concentration along the interface. The concentration gradients at the interface are very large, as a result, the variation of the concentration at the interface far exceeds that in the bulk.

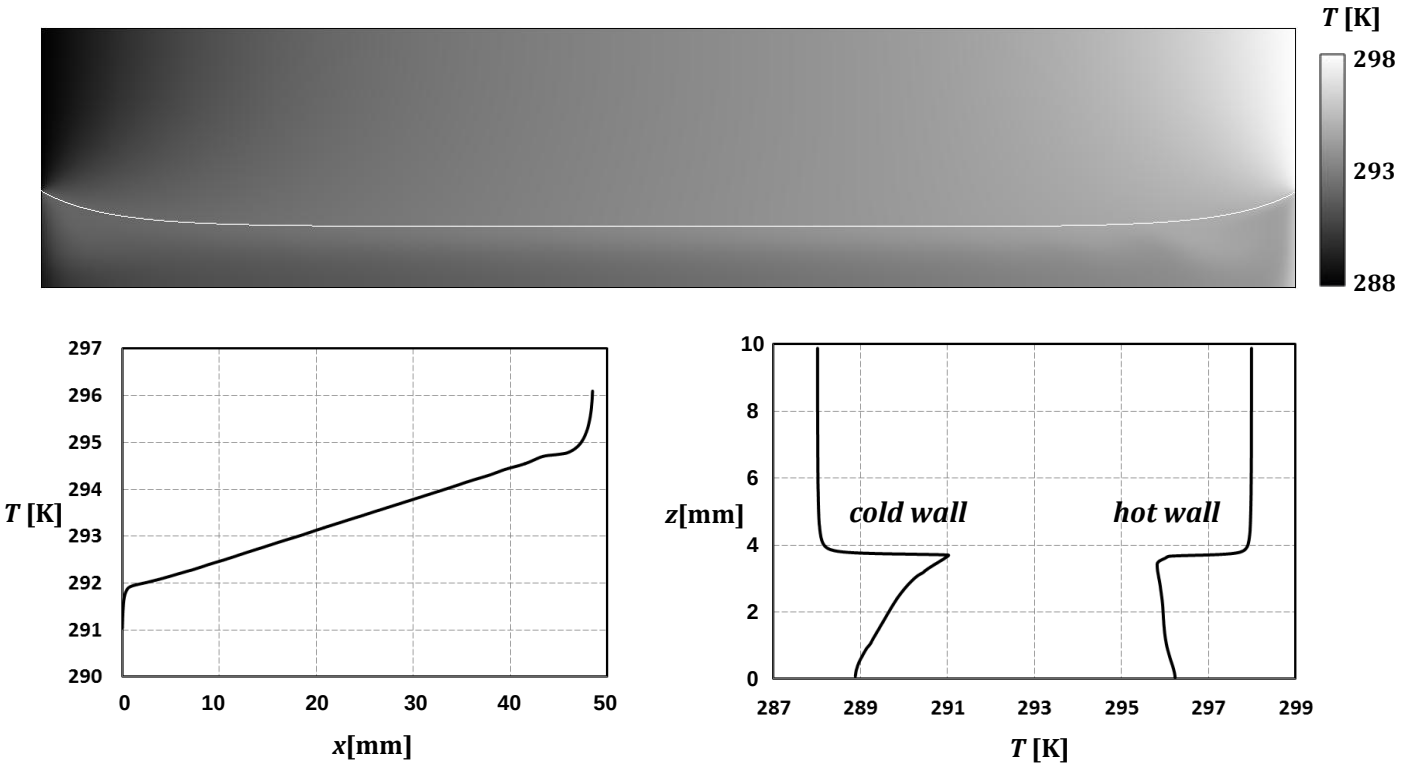

Figure 6 The temperature field for the water-methanol binary liquid and its vapors in the presence of air at atmospheric pressure. The entire cavity is shown in the upper panel. The thin white line shows the position of the liquid-vapor interface. The temperature distributions along the interface [lower left panel] and along the side walls [lower right panel] are also shown.

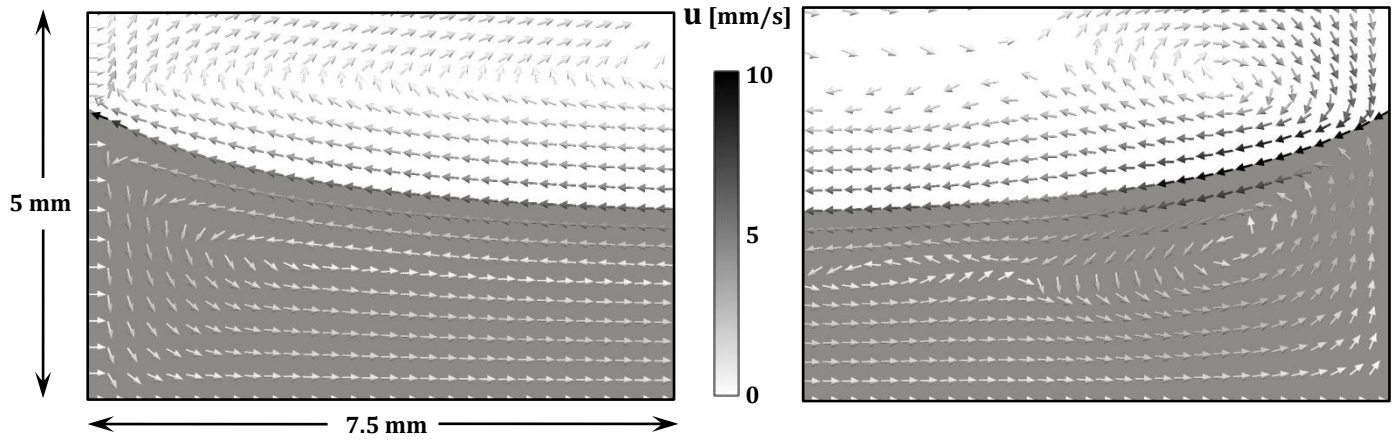

Figure 7 The liquid- and vapor-phase velocity fields for the binary liquid with isothermal composition of 90 mol% methanol and 10 mol% water in the presence of air at atmospheric pressure. The panels show the cooled [left] and heated [right] ends of the cavity. The gray background indicates liquid, the white background – vapor.